Classification: Physical Sciences (major), Applied Physical Sciences (minor)

Title: Stability of the A15 Phase in Diblock Copolymer Melts

Morgan W. Bates,[†,^] Joshua Lequieu,[†,^] Stephanie M. Barbon,[†] Ronald M. Lewis, III,[‖] Kris T. Delaney,[†] Athina Anastasaki,[†] Craig J. Hawker,[†,‡] Glenn H. Fredrickson,[§,†] and Christopher M. Bates*[,‡,§,†]

[^] These authors contributed equally

* To whom correspondence should be addressed: cbates@ucsb.edu, 805-893-5383

[†]Materials Research Laboratory, [‡]Department of Materials, and [§]Department of Chemical Engineering, University of California, Santa Barbara, California 93106, United States, [‖]Department of Chemical Engineering and Materials Science, University of Minnesota, Minneapolis, Minnesota 55455, United States

Keywords: block copolymer, topological close packing, tetrahedral close packing, A15 phase

ABSTRACT

The self-assembly of block polymers into well-ordered nanostructures underpins their utility across fundamental and applied polymer science, yet only a handful of equilibrium morphologies are known with the simplest AB-type materials. Here, we report the discovery of the A15 sphere phase in single component diblock copolymer melts comprising poly(dodecyl acrylate)–*block*–poly(lactide). A systematic exploration of phase space revealed that A15 forms across a substantial range of minority lactide block volume fractions (f_L= 0.25–0.33) situated between the σ sphere phase and hexagonally close-packed cylinders. Self-consistent field theory rationalizes the thermodynamic stability of A15 as a consequence of extreme conformational asymmetry. The experimentally observed A15–disorder phase transition is not captured using mean-field approximations but instead arises due to composition fluctuations as evidenced by fully fluctuating complex Langevin simulations. This combination of experiments and field-theoretic simulations provides rational design rules that can be used to generate unique, polymer-based mesophases through self-assembly.

SIGNIFICANCE STATEMENT

Block copolymers are prevalent throughout industry and academe due to their self-assembly into well-ordered nanostructures, but only a handful of morphologies are known with the simplest materials built from two chemically-distinct blocks. In this manuscript, we report that AB diblock copolymers can also self-assemble into a structure known as the A15 phase. Theory and experiments indicate A15 occurs throughout a substantial region of phase space with suitable differences in the space-filling characteristics of each block. The observed temperature-dependent phase transitions can only be explained using fully-fluctuating field theoretic simulations, which provide the first evidence that composition fluctuations play a key role in the self-assembly of block copolymers into the larger class of tetrahedrally close-packed sphere phases.

MAIN TEXT

Introduction

Atoms, molecules, and higher-order aggregates organize across vast length scales into structures that dictate the physical properties of all matter, from periodic crystalline solids to amorphous glasses. The importance of this connection between structure and properties is exemplified by a class of materials known as block copolymers. Covalently tethering immiscible polymers together results in spontaneous self-assembly on the nanometer length scale due to a competition between the unfavorable entropy loss of chain stretching and enthalpy of block–block interactions (1). The simplest and arguably most useful design involves two chemical constituents (A and B) arranged into diblock (AB), triblock (ABA), or longer alternating (ABABA…) sequences, all of which exhibit similar phase diagrams (2). By carefully choosing molecular connectivity, A and B chemistry, and morphology, block copolymers can produce tough engineering plastics (3) and elastomers (4), circumvent the optical diffraction limit for next-generation lithographic patterning (5), and support ion conduction in safe battery electrolytes (6) among other contemporary opportunities (7).

Given the breadth of materials applications that rely on microphase separation to furnish properties of interest, perhaps surprisingly, the phase behavior of AB-type block copolymers is severely restricted. The handful of classical morphologies include body-centered cubic (BCC) spheres, hexagonally close-packed (HCP) cylinders, interpenetrating gyroid networks (GYR), and alternating sheets of lamellae (LAM) (8). Additional phases, for example the O^{70} network (9) and face-centered cubic (FCC) spheres (10), have been sporadically observed in minute portions of the phase diagram, but these primarily remain academic curiosities since they are so difficult to access. Note that the limited palette of structures available with archetypal AB-type block copolymers

stands in glaring contrast to most other forms of hard and soft matter, for example metals, ceramics, and liquid crystals (11, 12).

Recent experiments with compositionally asymmetric diblock copolymer melts (A-block volume fractions $f_A << ½$) have identified equilibrium (σ) (13) and non-equilibrium (C14, C15) (14) structures that belong to a fascinating class of low symmetry sphere phases exhibiting tetrahedral (i.e., topological) close-packing (TCP). In a TCP phase, each atom or self-assembled (roughly spherical) particle is arranged with 12, 14, 15, or 16 neighbors that together form a triangulated coordination shell enveloping a polyhedron, the ensemble of which fills space (15). Depending on the crystal system and layer stacking, a staggering number of structures can be constructed and rationalized using this conceptual framework (16). One of the simplest TCP phases, known by the Strukturbericht designation A15 (alternatively, Pearson symbol *cP*8), contains two types of particles (coordination numbers CN = 12, 14) that decorate a cubic lattice. The A15 phase is prevalent throughout materials science. First observed in 1931 with β–tungsten (17), it has also been found in alloys (e.g., V_3Si, Nb_3Sn) (18) and a host of self-assembling soft materials including thermotropic (19) and lyotropic (20) liquid crystals, giant molecular tetrahedra (21) and surfactants (22), amphiphilic dendrons (23), and idealized soap froths (24). In contrast, A15 remains exceptionally rare in the field of block polymers. Park observed A15 in a blend of ionic liquids with charge-tethered diblock copolymers (25) leading to improved ion transport relative to other common phases (26). Mahanthappa also recently observed A15 in a hydrated AB diblock oligomer (27). Chanpuriya studied a more complex ABA′C tetrablock terpolymer sequence that transiently formed A15 on heating within a small window at elevated temperature, although this phase transition was irreversible upon cooling (28). We are unaware of any other experimental reports describing the A15 structure in block copolymer-based materials, which is

rather surprising. Groundbreaking theory by Grason dating back to 2003 predicted the stability of A15 in non-linear architectures (29), including AB_n "miktoarm" stars (30). The effect of such "architectural asymmetry" bears close similarities with "conformational asymmetry" that occurs, even in linear polymers, when blocks have different statistical segment lengths (31). Since conformational asymmetry has been implicated by Shi (32) and Schulze (33) as the key ingredient that favors the σ phase in diblock copolymers, presumably it should also stabilize A15. Yet, to the best of our knowledge A15 has not been found in diblock copolymer melts. Here, we demonstrate using a combination of experiments and theory that the A15 phase is in fact thermodynamically stable in AB diblock copolymer melts and can be found throughout a substantial region of phase space subject to appropriate molecular design.

Results

Self-consistent field theoretic (SCFT) simulations of AB diblock copolymer melts indicate A15 is indeed favored at large values of conformational asymmetry as parameterized by $\varepsilon = a_A/a_B$, where a_i represents the statistical segment length of block i (with segments defined to have equivalent volumes (34); Fig. 1). This metric accounts for chemistry-dependent differences in the pervaded volume of each block (Fig. 1, right) and is known to significantly impact phase behavior in other contexts, including the location of order–order transitions (35) and aforementioned emergence of the σ phase (33). Our calculations predict that for sufficiently large values of conformational asymmetry ($\varepsilon \gtrsim 2.1$), the A15 phase should appear across a wide range of volume fractions centered near $f_A = 0.3$ amid well-established σ and HEX morphologies. Presumably, A15 has not been observed in this region of phase space because the requisite (large) value of ε is non-trivial to achieve. We therefore sought to design suitable diblock copolymers with adequate

differences in a_i and initially targeted poly(dodecyl acrylate)–*block*–poly(lactide) (denoted DL). At fixed degree of polymerization N, the bulky poly(dodecyl acrylate) (PDDA) side-chain positions a significant fraction of the monomer volume pendent to the molecular backbone, which should reduce its statistical segment length (36) relative to poly(lactide) (PLA) with a_L = 7.9 Å at 25 °C (37). One would also anticipate this monomer pair exhibits a large Flory–Huggins interaction parameter χ that will promote self-assembly at low N, thereby facilitating the kinetics of self-assembly.

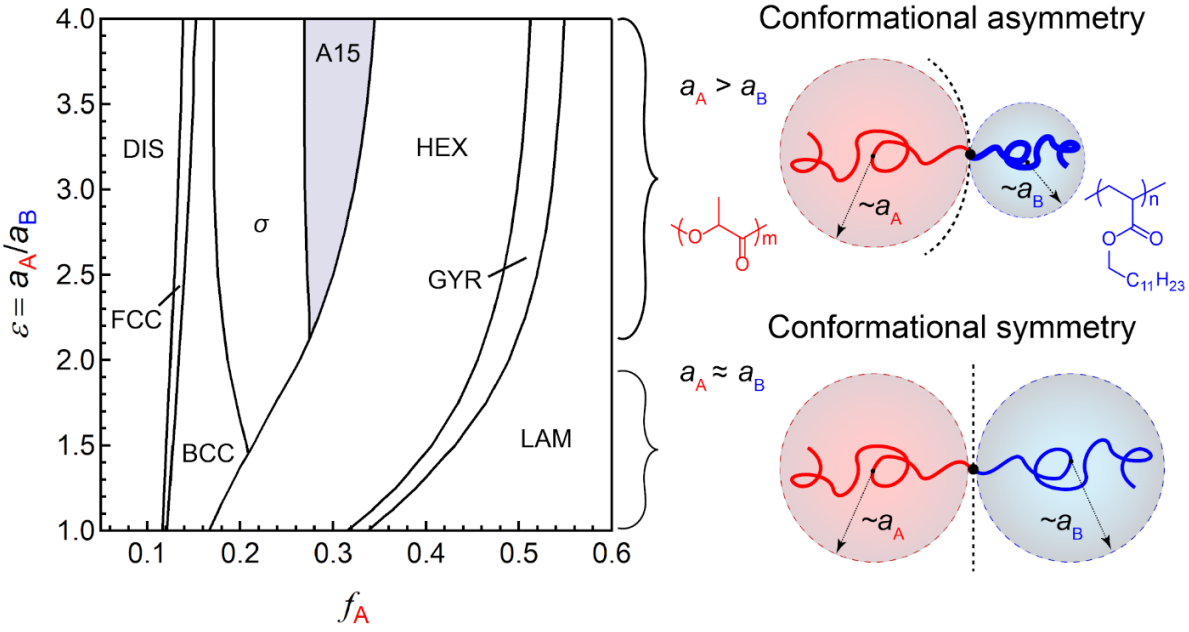

Fig. 1: *Left*: SCFT simulations (χN = 40) predict the A15 phase will be favored in AB diblock copolymers with sizeable conformational asymmetry, $\varepsilon \gtrsim 2.1$. *Right*: Illustration of the difference in pervaded block volumes that leads to large ε; poly(dodecyl acrylate)–*block*–poly(lactide) accentuates this effect.

A library of DL diblocks with low molar mass dispersities ($Đ < 1.10$) and varying PLA content (volume fractions $f_L = 0.15–0.82$) was therefore synthesized via sequential atom-transfer radical polymerization and ring-opening polymerization from 2-hydroxyethyl 2-bromoisobutyrate (Schemes S1–S2, Figs. S1–S8, Table S1). Guided by our SCFT predictions, we first focus on the self-assembly behavior of one sample, denoted DL–120 ($f_L = 0.29$), with a volumetric degree of polymerization $N = 120$. Small angle X-ray scattering (SAXS) experiments on DL–120 annealed at 125 °C for 19 hours reveal 24 well-defined Bragg reflections that are entirely consistent with those allowed by space group $Pm\bar{3}n$ (#223, Fig. 2a) (38). This number of peaks is sufficient to accurately reconstruct the unit cell electron density distribution by extracting structure factor amplitudes via Le Bail refinement (Fig. S9) and charge flipping to determine the corresponding phases (see supplementary information for details). Fig. 2b shows the result expressed at a 78% isosurface level; this structure is the A15 phase. Two characteristic types of micelles that are distinguished by their shape, volume, and coordination number occupy Wyckoff positions 2*a* and 6*d* (false colored green and purple, respectively). Both should be comprised of a PLA core since it is the minority component ($f_L = 0.32 < 0.50$), although this cannot be definitively determined from electron density maps (Fig. S10) due to the Babinet reciprocity principle. PDDA blocks fill all remaining space within the unit cell, left uncolored in Fig. 2b for clarity. See the supplementary information (Fig. S11) for representations of the coordination polyhedra with CN = 12 (position 2*a*) and CN = 14 (6*d*). Fig. 2c highlights the characteristic tiling found in layers perpendicular to each *a*-axis (as depicted, in a {100} plane). A slight departure from regular hexagons and triangles is required to square the net and accommodate cubic lattice symmetry (16). Two different nodes are present — $3^2.6^2$ (black circles) and 3.6.3.6 (white circles).

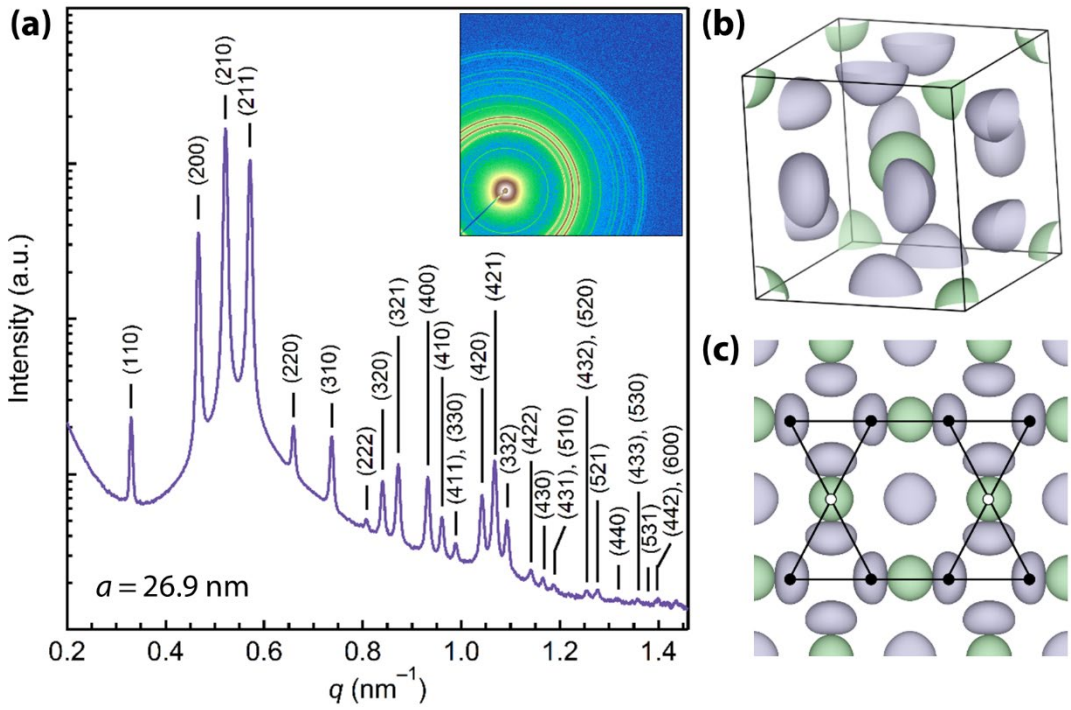

Fig. 2: Discovery of the A15 phase in DL diblock copolymers. **(a)** SAXS profile of A15 obtained with DL–120 (annealed at 125 °C for 19 hours); all allowed reflections for space group $Pm\bar{3}n$ out to (600) are demarcated with vertical lines (a = 26.9 nm). **(b)** Unit cell electron density reconstruction (78% isosurface) corresponding to the data in (a); see supplementary information for details. Two symmetry-distinct micelles (shape, volume) occupy Wyckoff positions 2*a* and 6*d* (false colored green and purple, respectively). **(c)** Projection of the electron density map along one *a*-axis with an outline of the characteristic A15 tiling pattern containing two types of nodes — $3^2.6^2$ (black circles) and 3.6.3.6 (white circles).

To probe the stability of A15 as a function of temperature, a second sample (DL–76, f_L = 0.31) was prepared with a similar volume fraction as DL–120 but lower overall N = 76. This results in a reduction of the order–disorder transition temperature (T_{ODT}) to a more accessible value of 105 °C as measured by oscillatory rheology (Fig. S7). Dynamic SAXS experiments conducted on

heating and cooling through T_{ODT} show fast and reversible formation of A15 (Fig. 3a), suggesting it is indeed thermodynamically favored. Extended isothermal treatment of this A15 phase at 70 °C for 4–5 days results in no change to the position or intensity of scattering peaks (Fig. S12). Similar analyses conducted as a function of volume fraction and temperature ($\chi \sim 1/T$) for DL samples spanning $f_L = 0.15–0.82$ were used to construct the equilibrium phase diagram depicted in Fig. 3b; the temperature dependence of χ was estimated by fitting SAXS data collected on a disordered DL sample to the random phase approximation structure factor (see Figs. S13–14 and accompanying discussion). A15 is situated at volume fractions intermediate to σ and HEX over the approximate range $f_L = 0.25–0.33$. Pure A15 can be isolated except at the boundaries, where σ/A15 or A15/HEX phase coexistence is observed. Coexistence may be a consequence of the pseudo-single-component nature of all block polymers prepared by controlled polymerization techniques. While the dispersity in molar mass for DL samples is low ($Đ < 1.1$), the inevitable mixture of species implies Gibbs' phase rule would permit coexistence at constant temperature and pressure.

The corresponding phase diagram computed via SCFT for $\varepsilon = 3$ (Fig. 3c) demonstrates good agreement with experiments for $\chi N > 30$ in both the relative position of phases and the approximate range of volume fractions over which they occur. Moreover, the shape and size of micelles in the A15 structure matches experiments (Fig. S15), including significant deformation observed at Wyckoff position 6*d*. For $\chi N < 30$ however, SCFT predictions do not agree with experiments. Whereas SAXS data indicate A15 forms directly from a disordered melt (Fig. 3a, Fig. 3b filled symbols), SCFT anticipates the system should instead traverse a phase sequence DIS–BCC–σ–A15 on cooling. We argue this discrepancy is due to composition fluctuations that

are neglected by the mean-field SCFT treatment, which emerge in finite molecular weight polymers and can disrupt ordered phases near T_{ODT} (39).

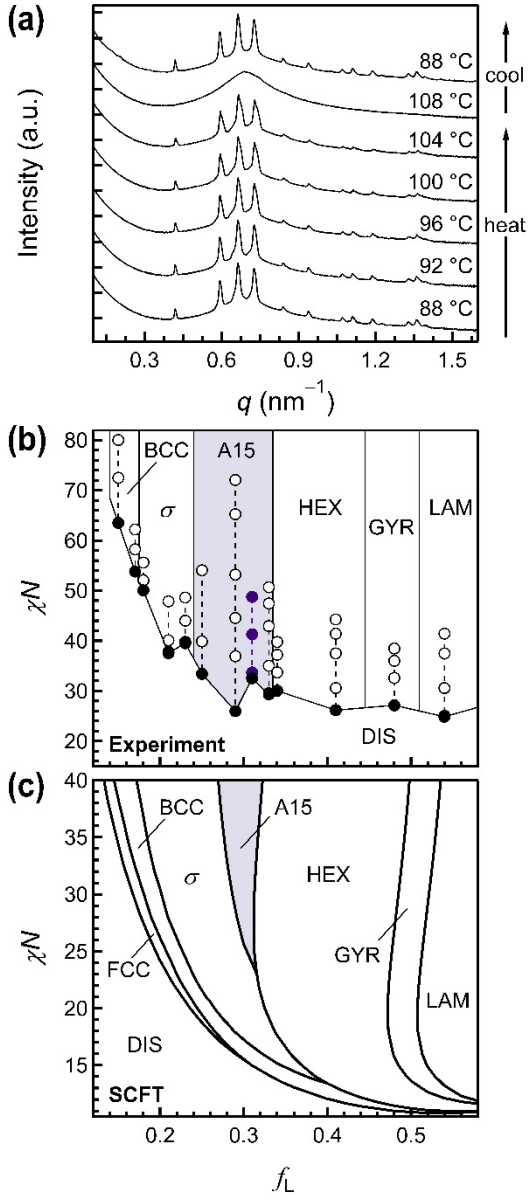

Fig. 3: Phase behavior of DL diblock copolymers. **(a)** A15 forms reversibly in DL–76 as evidenced by dynamic heating (1 °C/min) and cooling through the order–disorder transition temperature ($T_{ODT} \approx 105$ °C). **(b)** The experimental DL phase diagram reveals a region of A15

stability circa f_L = 0.25–0.33; phase coexistence (σ/A15 and A15/HEX) occurs near either f_L boundary. Points examined by SAXS are marked with open circles and $(\chi N)_{ODT}$ identified with dynamic mechanical thermal analysis is indicated by filled black circles. Sample DL–76 from (a) is denoted with filled purple circles. **(c)** SCFT mean-field phase diagram mapped onto χN vs. f_L at $\varepsilon = 3$ semi-quantitatively matches experiments: σ, A15, and HEX phases occur over similar volume fraction ranges at large χN. The disagreement for $\chi N < 30$ arises due to composition fluctuations as addressed in Fig. 4 (see text for discussion).

To account for composition fluctuations, fully fluctuating field theoretic simulations (FTS) were used to calculate the free energy (40) of A15 and σ phases in the vicinity of T_{ODT}. Note that microphase separation in the models suitable for FTS is governed by a new segregation strength parameter (α) that can be related to χN through established procedures (40, 41). Determining fluctuation-corrected free energies represents a major computational challenge previously not attempted for TCP phases consisting of large unit cells like A15 and σ. These calculations necessitate careful simulation design to resolve the miniscule free energy difference that separates the A15 and σ phases ($\approx 10^{-4}\ k_B T$ per chain by SCFT estimates). Nevertheless, we have overcome these obstacles; the FTS simulations indicate compositional fluctuations invert the stability of A15 and σ (Fig. 4, see supplementary information for details). In contrast to SCFT, which predicts σ is favored for $\alpha < 29$ near the mean-field order–disorder transition (Fig. 4a), fluctuations stabilize A15 for all values of $\alpha > \alpha_{ODT}$ (Fig. 4b). To the best of our knowledge, this is the first computational evidence that composition fluctuations regulate the formation and stabilization of TCP phases in any type of block polymer melt.

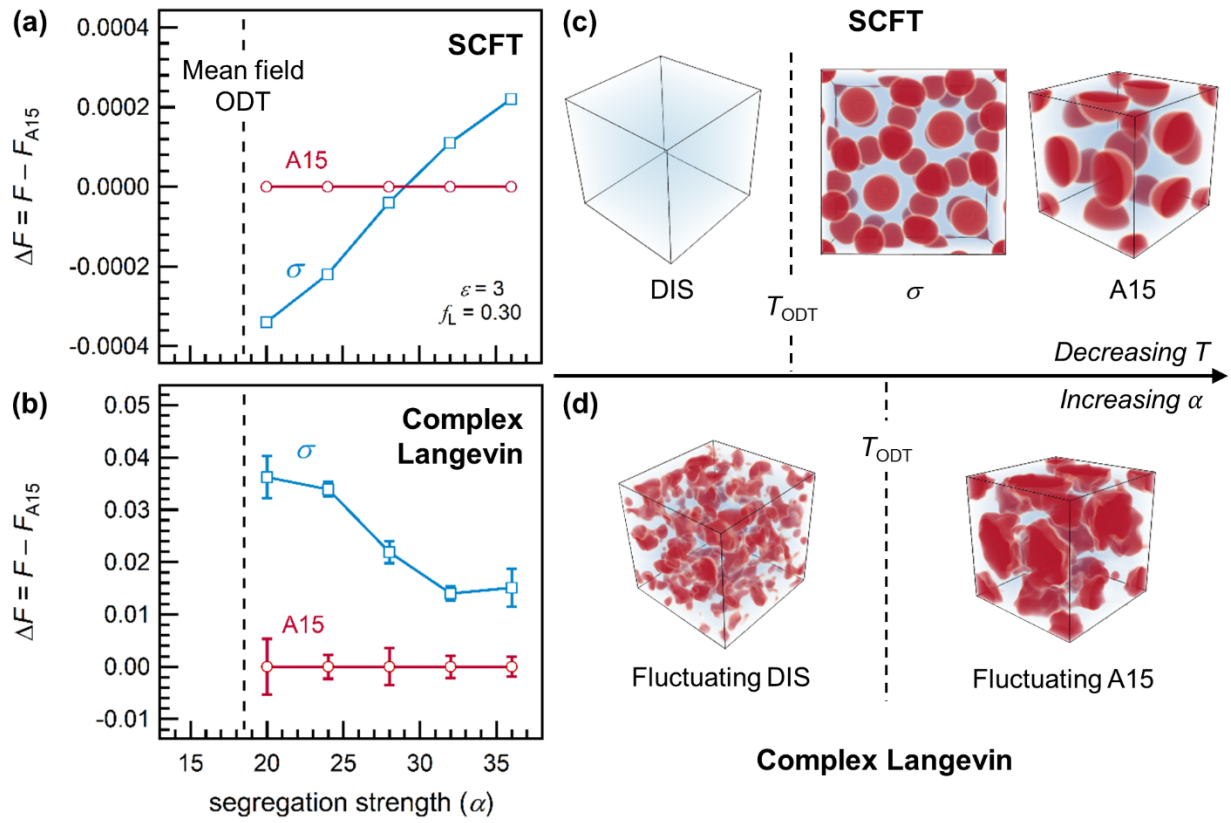

Fig. 4: Relative stability of the A15 and σ phases (free energy per chain differences) as calculated with **(a)** SCFT and **(b)** fully fluctuating field-theoretic simulations for $f_L = 0.3$ and invariant degree of polymerization $\bar{N} = 5400$. Segregation strength in the model used for both SCFT and FTS is controlled by the parameter α, which is related to χN. **(c, d)** Unit cell renderings from **(c)** SCFT and **(d)** FTS highlight the different predicted temperature-dependent phase sequences, an effect of fluctuations; discrete, red domains are PLA-rich. Note that the BCC phase has been omitted from (c) for clarity.

Quantitative Comparison of Theory and Experiment

A quantitative comparison of theory and experiment necessitates knowledge of ε and thus the statistical segment lengths of PLA (a_L) and PDDA (a_D). While Anderson has reported the value of a_L from neutron scattering (37) and a variety of poly(acrylate) values are also available (42), we were unable to find any reports of a_D for poly(dodecyl acrylate). As described in the supplementary information, neutron scattering was therefore used to measure a_D by fitting absolute intensity data to the random phase approximation structure factor for blends of hydrogenous and deuterated homopolymers (Tables S3–S4, Figures S16–S17). We find a_D = 4.3 Å at 25 °C with a reference volume (v_0) of 118 Å^3 that was also used to normalize all of the statistical segment lengths in the following discussion. This value of a_D follows the expected decreasing trend for poly(acrylates) with increasing alkyl side-chain length, and it is significantly smaller than reported values for poly(ethyl acrylate) (6.1 Å) and poly(octyl acrylate) (5.5 Å) (42). In comparison, a_L = 7.9 Å at 25 °C as extrapolated from the temperature (T) dependence d(ln R_g)/dT (37), where R_g is the unperturbed radius of gyration. For DL diblock copolymers, $\varepsilon = a_L/a_D$ is therefore approximately 1.85. Before drawing comparisons to other materials reported in the literature, note that two conventions exist for defining ε, where it either scales as a_A/a_B or $(a_A/a_B)^2$; herein, the former is exclusively used.

Schulze and coworkers (33) synthesized a series of three diblock copolymers with varying conformational asymmetry and found that the region of σ phase stability increases significantly for the largest ε = 1.3 corresponding to poly(ethylethylene)–*block*–poly(lactide) (PEE–PLA). Swapping out the PEE block for PDDA evidently further amplifies ε, causing A15 to become stable. Interestingly, the volume fraction at which PEE–PLA undergoes a phase transition from σ

to HEX occurs circa f_L = 0.24, which is approximately the value we observe for the σ–A15 boundary found in Fig. 3. The simulations in Fig. 1 anticipate this σ–A15 transition is relatively insensitive to ε but the σ–HEX curve should shift towards higher f_L as ε increases.

The experimentally measured value of ε (1.85) for DL diblock copolymers is large compared to other reported materials but still smaller than the critical value needed to stabilize the A15 phase as predicted by theory (ε_c = 2.1, Fig. 1). Although the origin of this inconsistency is unclear, it agrees with other literature involving block copolymer melts. In general, SCFT simulations based on thread-like continuous Gaussian chain models overestimate the value of ε required to stabilize complex sphere phases. For example, Xie et al. predict the σ phase occurs across a tiny sliver of phase space spanning $\Delta f_A < 0.02$ when $\varepsilon = 1.5$ (32), yet experiments find the window is circa 0.06 with a smaller ε of 1.3 (33). Moreover, the results in Fig. 1 indicate σ should not be stable when $\varepsilon \lesssim 1.4$, but experiments have found it in poly(isoprene)–*block*–poly(lactide) with $\varepsilon = 1.15$ (33). We therefore consider the agreement between experiments and theory relatively good in the present context. Given the lack of a one-to-one correspondence between theoretical and experimental ε values, the breadth of the A15 channel observed in Fig. 3b (≈10 vol%) is more consistent with a theoretical $\varepsilon > 3$ (c.f., Fig. 1).

Origins of A15 Stability

Block polymer self-assembly is governed by a delicate balance of two competing energetic effects — interfacial energy and loss of conformational entropy due to chain stretching — that play a crucial role in the selection of various sphere phases (43). Why does A15 form in linear

diblock copolymers at large volume fractions and low temperatures (high χN)? At first glance, it is tempting to attribute both facts to the famous Kelvin foam problem, which asks what partition of space *into equal volume cells* minimizes interfacial area. For about 100 years, the solution was thought to be a truncated octahedron (the Wigner–Seitz cell of body-centered cubic spheres). In 1994, Weaire and Phelan provided a counterexample: the Wigner–Seitz polyhedra of an A15 unit cell constrained to equal volumes — two pentagonal dodecahedra and six tetrakaidodecahedra (44). A convenient measure of shape sphericity that captures this trend is the isoperimetric quotient, $\mathrm{IQ} = 36\pi V^2/A^3$, where V is volume, A is surface area, and IQ = 1 represents a sphere. Associating one IQ with an entire unit cell by averaging over all constituent (equal volume) polyhedra yields $\mathrm{IQ}_{\mathrm{BCC}} = 0.7534 < \mathrm{IQ}_{\mathrm{A15}} = 0.764$, which implies A15 is more spherical than BCC. The nominal connection with block polymer self-assembly involves the shape of micelles (core + corona) and their cores that are bounded by the block–block interface. As f_{A} grows within a lattice of constant dimensions, the shape of micellar cores will deform as they impinge upon local Wigner–Seitz cells. This polyhedral distortion is opposed by an energetic preference to maintain spherical A–B interfaces. Thus, the Weaire–Phelan solution seemingly suggests that A15 should be selected over other morphologies at large f_{A} (Fig. 3) to produce, on average, the most spherical micellar cores when polyhedral distortion is unavoidable. The same effect would then also rationalize the stability of A15 at low temperatures (Fig. 3); sharper block–block interfaces favor more spherical micellar cores (45). However, there is a subtle but important difference between the Kelvin foam problem and the present situation: in the actual A15 mesophase (Fig. 2), Wigner–Seitz cells *are not equal volume* (46).

Lee et al. recently relaxed the equal volume constraint by calculating IQ values using the Voronoi domains of a given crystal (45). Their analysis revealed that the σ phase (5 types of

polyhedra in a unit cell) is then surprisingly more spherical than A15: $IQ_{A15} = 0.7618 < IQ_{\sigma} = 0.7624$. Grason has further shown that other TCP phases (e.g., C14 and C15) also beat A15 in terms of interfacial area minimization (43). We therefore argue that micellar core sphericity alone cannot explain the stability of A15 at large f_A and low temperatures. This is reinforced by analysis of our SCFT simulations. The average IQ of micellar cores (as defined by $f_A = f_B = 0.5$ isosurfaces) within a unit cell is always more spherical in σ than A15 across all volume fractions $f_A = 0.15$–0.35 ($\varepsilon = 3$, $\chi N = 40$; Fig. S18a) and segregation strengths $\chi N = 15$–40 ($\varepsilon = 3$, $f_A = 0.3$; Fig. S18b). There is no obvious crossover that would signify a phase transition and the difference between σ and A15 actually grows with f_A and χN. Another interesting observation is that every IQ > 0.95, suggesting the micellar cores inherit rather minimal polyhedral distortion from their Wigner–Seitz cells at the relevant volume fractions and segregation strengths. We conclude that a subtle balance between block–block interfacial area and chain stretching effects likely stabilizes A15, as has been invoked previously to explain the prevalence of σ (43).

Fluctuation Effects

Fluctuations have long been known to impose significant effects on the self-assembly of block copolymers near the order–disorder transition (ODT). Perhaps the best known example is the phase diagram of poly(isoprene)–*block*–poly(styrene), which experimentally looks quite different from SCFT predictions at low segregation strengths (47). The role of fluctuations in diblocks has been theoretically analyzed by a variety of analytic (39, 48) and numerical (40, 49) techniques that collectively indicate microphase destabilization and a corresponding shift in T_{ODT} to lower temperatures. This effect truncates the mean-field (SCFT) phase diagram, resulting in

direct transitions from the disordered state into ordered phases like cylinders or gyroid without first traversing BCC as predicted by SCFT (as in Fig. 3c).

Though these general trends are seen in our fluctuation-corrected free energies shown in Fig. 4, several distinct differences deserve comment. First, the results in Fig. 4b indicate fluctuations stabilize A15 over σ *irrespective* of the fluctuation-induced shift in T_{ODT} — σ is higher in free energy across the entire range of α values (at $f_A = 0.3$ and $\varepsilon = 3$). Moreover, our calculations suggest that although both ordered phases are metastable in this regime (relative to the disordered phase), A15 is thermodynamically favored over σ. Since the formation of TCP phases in block copolymers can strongly depend on the nucleation pathway from the disordered state, particularly for TCP phases often separated by small free energy differences (14), the fluctuation-induced stability of A15 over σ in the disordered melt might aid in its nucleation versus other TCP or classical phases.

Second, we note that the free energy differences reported in Fig. 4 between A15 and σ are two orders of magnitude smaller in SCFT ($\approx 2x10^{-4}$ kT/chain) than the fluctuation-corrected values ($\approx 2x10^{-2}$ kT/chain). To date, block copolymer TCP phases have only been observed in low molecular weight molecules, suggesting that perhaps they emerge as a consequence of favorable kinetics: short chains can diffuse more quickly, thereby facilitating the formation of characteristically large unit cells. Our results augment this kinetic argument by suggesting that short chains also have *thermodynamic* consequences. Fluctuations associated with finite length evidently increase the thermodynamic driving force towards A15 (at $f_A = 0.3$, $\varepsilon = 3$) and could plausibly influence other TCP phases as well. The optimal phase that arises due to fluctuations likely also depends on volume fraction and conformational asymmetry. Note that these conclusions

are consistent with other recent experimental work suggesting fluctuation effects explain the occurrence of σ only below the entanglement molecular weight (50).

Conclusions

In summary, AB diblock copolymer melts can self-assemble into the A15 phase. Experiments and theory have systematically mapped out phase diagrams for poly(dodecyl acrylate)–*block*–poly(lactide) that locate A15 near f_L = 0.25–0.33, situated between σ and HEX. Extended isothermal annealing and dynamic heating/cooling experiments through the order–disorder transition temperature suggest A15 is an equilibrium structure, and theory implicates conformational asymmetry as a key design parameter that promotes its formation. A direct and reversible A15–disorder phase transition is stabilized by composition fluctuations as supported by fully fluctuating field-theoretic simulations, suggesting they are an important factor in the selection of various tetrahedrally close-packed block polymer structures. These results provide rational design rules that expand the limited set of mesophases accessible via equilibrium block polymer self-assembly.

MATERIALS AND METHODS

Full synthetic methods and simulation details are provided in the supplementary information. Poly(dodecyl acrylate)–*block*–poly(lactide) samples were synthesized via sequential atom-transfer radical polymerization and ring-opening polymerization from 2-hydroxyethyl 2-bromoisobutyrate. Polymers were characterized by ^{1}H NMR spectroscopy, size-exclusion chromatography, MALDI-ToF mass spectrometry, differential scanning calorimetry, and thermal

gravimetric analysis. Temperature-dependent small angle X-ray scattering experiments were performed at the DND-CAT 5-ID-D beamline of the Advanced Photon Source (Argonne National Laboratory, Argonne, IL). SAXS samples were prepared in DSC pans and sealed under N_2 in a glove box. SAXS data reduction and unit cell electron density reconstruction procedures are described in the supplementary information. SCFT and fully-fluctuating complex Langevin simulations were performed on the UCSB supercomputer cluster in the California NanoSystems Institute. All data discussed in the paper is available in the manuscript and supplementary materials.

REFERENCES AND NOTES

1. Bates FS (1991) Polymer--Polymer Phase Behavior. *Science* 251(4996):898–905.

2. Matsen MW (2012) Effect of Architecture on the Phase Behavior of AB-Type Block Copolymer Melts. *Macromolecules* 45(4):2161–2165.

3. Bates FS, Fredrickson GH, Hucul D, Hahn SF (2004) PCHE-Based Pentablock Copolymers: Evolution of a New Plastic. *AIChE J* 47(4):762–765.

4. Drobny JG (2014) Styrenic Block Copolymers. *Handbook of Thermoplastic Elastomers, Second Edition* (Elsevier Inc.), pp 175–194.

5. Bates CM, Maher MJ, Janes DW, Ellison CJ, Willson CG (2014) Block Copolymer Lithography. *Macromolecules* 47(1):2–12.

6. Hallinan DT, Balsara NP (2013) Polymer Electrolytes. *Annu Rev Mater Res* 43(1):503–525.

7. Bates CM, Bates FS (2017) 50th Anniversary Perspective: Block Polymers---Pure Potential. *Macromolecules* 50(1):3–22.

8. Cochran EW, Garcia-Cervera CJ, Fredrickson GH (2006) Stability of the Gyroid Phase in Diblock Copolymers at Strong Segregation. *Macromolecules* 39(7):2449–2451.

9. Takenaka M, et al. (2007) Orthorhombic Fddd Network in Diblock Copolymer Melts. *Macromolecules* 40(13):4399–4402.

10. Huang Y-Y, Hsu J-Y, Chen H-L, Hashimoto T (2007) Existence of fcc-Packed Spherical Micelles in Diblock Copolymer Melt. *Macromolecules* 40(3):406–409.

11. De Graef M De, McHenry ME (2012) *Structure of Materials* (Cambridge University Press).

12. Sun H-J, Zhang S, Percec V (2015) From Structure to Function via Complex Supramolecular Dendrimer Systems. *Chem Soc Rev* 44(12):3900–3923.

13. Lee S, Bluemle MJ, Bates FS (2010) Discovery of a Frank--Kasper σ Phase in Sphere-Forming Block Copolymer Melts. *Science* 330(6002):349–353.

14. Kim K, et al. (2017) Thermal Processing of Diblock Copolymer Melts Mimics Metallurgy. *Science* 356(6337):520–523.

15. Frank FC, Kasper JS (1958) Complex Alloy Structures Regarded as Sphere Packings. I. Definitions and Basic Principles. *Acta Crystallogr* 11(3):184–190.

16. Frank FC, Kasper JS (1959) Complex Alloy Structures Regarded as Sphere Packings. II. Analysis and Classification of Representative Structures. *Acta Crystallogr* 12(7):483–499.

17. Hartmann H, Ebert F, Bretschneider O Elektrolysen in Phosphatschmelzen. I. Die Elektrolytische Gewinnung von α- und β-Wolfram. *Zeitschrift für Anorg und Allg Chemie* 198(1):116–140.

18. Muller J (1980) A15-Type Superconductors. *Reports Prog Phys* 43(5):641.

19. Balagurusamy VSK, Ungar G, Percec V, Johansson G (1997) Rational Design of the First Spherical Supramolecular Dendrimers Self-Organized in a Novel Thermotropic Cubic Liquid-Crystalline Phase and the Determination of Their Shape by X-ray Analysis. *J Am Chem Soc* 119(7):1539–1555.

20. Perroni D V., Mahanthappa MK (2013) Inverse Pm-3n Cubic Micellar Lyotropic Phases from Zwitterionic Triazolium Gemini Surfactants. *Soft Matter* 9:7919–7922.

21. Huang M, et al. (2015) Selective Assemblies of Giant Tetrahedra via Precisely Controlled Positional Interactions. *Science* 348(6233):424–428.

22. Yue K, et al. (2016) Geometry Induced Sequence of Nanoscale Frank--Kasper and Quasicrystal Mesophases in Giant Surfactants. *Proc Natl Acad Sci U S A* 113(50):14195–14200.

23. Cho B-K, Jain A, Gruner SM, Wiesner U (2004) Mesophase Structure-Mechanical and Ionic Transport Correlations in Extended Amphiphilic Dendrons. *Science* 305(5690):1598–1601.

24. Gabbrielli R, Meagher AJ, Weaire D, Brakke KA, Hutzler S (2012) An Experimental Realization of the Weaire–Phelan Structure in Monodisperse Liquid Foam. *Philos Mag Lett* 92(1):1–6.

25. Jung HY, Park MJ (2017) Thermodynamics and Phase Behavior of Acid-Tethered Block Copolymers with Ionic Liquids. *Soft Matter* 13:250–257.

26. Jung HY, Kim O, Park MJ (2016) Ion Transport in Nanostructured Phosphonated Block Copolymers Containing Ionic Liquids. *Macromol Rapid Commun* 37(14):1116–1123.

27. Jayaraman A, Zhang DY, Dewing BL, Mahanthappa MK (2019) Path-Dependent Preparation of Complex Micelle Packings of a Hydrated Diblock Oligomer. *ACS Cent Sci* ASAP. doi:10.1021/acscentsci.8b00903.

28. Chanpuriya S, et al. (2016) Cornucopia of Nanoscale Ordered Phases in Sphere-Forming Tetrablock Terpolymers. *ACS Nano* 10(5):4961–4972.

29. Grason GM, DiDonna BA, Kamien RD (2003) Geometric Theory of Diblock Copolymer Phases. *Phys Rev Lett* 91(5):58304.

30. Grason GM, Kamien RD (2004) Interfaces in Diblocks: A Study of Miktoarm Star Copolymers. *Macromolecules* 37(19):7371–7380.

31. Milner ST (1994) Chain Architecture and Asymmetry in Copolymer Microphases. *Macromolecules* 27(8):2333–2335.

32. Xie N, Li W, Qiu F, Shi A-C (2014) σ Phase Formed in Conformationally Asymmetric AB-Type Block Copolymers. *ACS Macro Lett* 3(9):906–910.

33. Schulze MW, et al. (2017) Conformational Asymmetry and Quasicrystal Approximants in Linear Diblock Copolymers. *Phys Rev Lett* 118(20):207801.

34. Bates FS, Fredrickson GH (1994) Conformational Asymmetry and Polymer-Polymer Thermodynamics. *Macromolecules* 27(4):1065–1067.

35. Matsen MW, Bates FS (1997) Conformationally Asymmetric Block Copolymers. *J Polym Sci Part B: Polym Phys* 35:945–952.

36. Bates FS, Fredrickson GH (1994) Conformational Asymmetry and Polymer--Polymer Thermodynamics. *Macromolecules* 27(4):1065–1067.

37. Anderson KS, Hillmyer MA (2004) Melt Chain Dimensions of Polylactide. *Macromolecules* 37(5):1857–1862.

38. Hahn T ed. (2005) *International Tables for Crystallography Volume A: Space-Group Symmetry* (Springer). 5th Ed.

39. Fredrickson GH, Helfand E (1987) Fluctuation Effects in the Theory of Microphase Separation in Block Copolymers. *J Chem Phys* 87(1):697–705.

40. Delaney KT, Fredrickson GH (2016) Recent Developments in Fully Fluctuating Field-Theoretic Simulations of Polymer Melts and Solutions. *J Phys Chem B* 120(31):7615–7634.

41. Glaser J, Medapuram P, Beardsley TM, Matsen MW, Morse DC (2014) Universality of Block Copolymer Melts. *Phys Rev Lett* 113(6):68302.

42. Mark JE ed. (2007) *Physical Properties of Polymers* (Springer Science + Business Media, LLC, New York, NY). 2nd Ed.

43. Reddy A, et al. (2018) Stable Frank-Kasper Phases of Self-Assembled, Soft Matter Spheres. *Proc Natl Acad Sci U S A* 115(41):10233–10238.

44. Weaire D, Phelan R (1994) A Counter-Example to Kelvin's Conjecture on Minimal Surfaces. *Philos Mag Lett* 69(2):107–110.

45. Lee S, Leighton C, Bates FS (2014) Sphericity and Symmetry Breaking in the Formation of Frank-Kasper Phases from One Component Materials. *Proc Natl Acad Sci U S A* 111(50):17723–17731.

46. Grason GM (2016) Frank Kasper Phases of Squishable Spheres and Optimal Cell Models. *J Club Condens Matt Phys*:1–3.

47. Khandpur AK, et al. (1995) Polyisoprene-Polystyrene Diblock Copolymer Phase Diagram near the Order-Disorder Transition. *Macromolecules* 28(26):8796–8806.

48. Qin J, Grzywacz P, Morse DC (2011) Renormalized One-Loop Theory of Correlations in Disordered Diblock Copolymers. *J Chem Phys* 135(8):84902.

49. Stasiak P, Matsen MW (2013) Monte Carlo Field-Theoretic Simulations for Melts of Symmetric Diblock Copolymer. *Macromolecules* 46(19):8037–8045.

50. Lewis RM, et al. (2018) Role of Chain Length in the Formation of Frank-Kasper Phases in Diblock Copolymers. *Phys Rev Lett* 121(20):208002.

ACKNOWLEDGMENTS

We thank Patrick Corona and Matt Helgeson for assistance with neutron scattering measurements. Portions of this work were performed at the DuPont-Northwestern-Dow Collaborative Access Team (DND-CAT) located at Sector 5 of the Advanced Photon Source (APS). DND-CAT is supported by Northwestern University, E.I. DuPont de Nemours & Co., and The Dow Chemical Company. This research used resources of the Advanced Photon Source, a U.S. Department of Energy (DOE) Office of Science User Facility operated for the DOE Office of Science by Argonne National Laboratory under Contract No. DE-AC02-06CH11357. Data were collected using an instrument funded by the National Science Foundation under Award Number 0960140.

Funding: This material is based upon work supported by the U.S. Department of Energy, Office of Basic Energy Sciences, under Award Number DE-SC0019001 (nanostructure characterization, scattering experiments, theory, simulations) and as part of the Center for Materials for Water and Energy Systems (M-WET), an Energy Frontier Research Center funded by the U.S. Department of Energy, Office of Science, Basic Energy Sciences under Award #DE-SC0019272 (synthesis and synthetic characterization). SMB and AA acknowledge Elings Fellowships through the California NanoSystems Institute. The research reported here made use of shared facilities of the UCSB MRSEC (NSF DMR 1720256), a member of the Materials Research Facilities Network (www.mrfn.org).

Authors contributions: The manuscript was written by MWB, JL, and CMB. Experiments were designed by MWB, SMB, CMB, and CJH. Synthetic procedures were optimized by MWB, SMB, and AA. Scattering experiments were performed by MWB and SMB. Rheology data were collected by MWB and RML. Simulations were designed by JL, KTD, and GHF and performed

by JL. Fits to RPA theory were performed by KTD and CMB. All authors have given approval to the final version of the manuscript.

Competing interests: The authors declare no competing financial interest.